Structure, branching ratios, and a laser-cooling scheme for the ^{138}BaF molecule

Tao Chen,* Wenhao Bu, and Bo Yan†
Department of Physics, Zhejiang University, Hangzhou, China, 310027
(Received 26 September 2016; published 19 December 2016)

For laser-cooling considerations, we have theoretically investigated the electronic, rovibrational, and hyperfine structures of the BaF molecule. The highly diagonal Franck-Condon factors and the branching ratios for all possible transitions within the lowest-lying four electronic states have also been calculated. Meanwhile, the mixing between the metastable $A'^2\Delta$ and $A^2\Pi$ states and, further, the lifetime of the Δ state have been estimated since the loss procedure via the Δ state might fatally break the main quasicycling $\Sigma - \Pi$ transition for cooling and trapping. The resultant hyperfine splittings of each rovibrational state in the $X^2\Sigma^+$ state provide benchmarks for sideband modulations of the cooling and repumping lasers and the remixing microwaves to address all necessary levels. The calculated Zeeman shift and g factors for both X and A states serve as benchmarks for selection of the trapping laser polarizations. Our study paves the way for future laser cooling and magneto-optical trapping of the BaF molecule.

DOI: 10.1103/PhysRevA.94.063415

I. INTRODUCTION

Ultracold polar molecules [1], due to the tunable long-range dipole-dipole interactions [2], provide access to many new potential regimes, such as novel many-body physics [3], ultracold chemistry [4], precision measurement [5,6], and quantum computation and information processing [7,8]. However, a big challenge is to produce quantum molecular samples (such as KRb [9–11]), i.e., achieve high phase-space density in an ultracold regime. Besides complicated indirect creation methods, direct Stark, Zeeman, and optoelectric slowing and cooling [12–17] can only yield molecular samples at millidegrees Kelvin temperature and, even worse, the phase-space density cannot be increased. Consequently, approaches of extending a widely used traditional laser-cooling technique in atoms to polar molecules are being explored [18–25] and, fortunately, laser-cooling and magneto-optical trapping experiments have recently been realized for particular species of molecules, including SrF [20,21], YO [22,23], and CaF [24,25]. Now other ongoing candidates, such as YbF [26], MgF [27], BH [28], RaF [29], TiF [30], and BaH [31], have attracted great interest as well.

For molecules, the much more complex internal rovibrational structures make finding a closed cycling transition required by laser cooling much more difficult than for atoms. Those laser-cooled molecules above share a common feature, i.e., highly diagonal Franck-Condon factors (FCFs), which results in a relatively simple quasicycling cooling scheme, that is, only two repumping lasers are required experimentally [21] to eliminate the undesired spontaneous decays to dark vibrational states. Besides the vibrational transitions, the rotational transitions could be closed by choosing the $|N = 1\rangle \leftrightarrow |N' = 0\rangle$ transitions, where the strict parity and angular momentum selection rules guarantee the pumped excited-state molecules entirely decay back to the $N = 1$ ground state [19]. Meanwhile, all of the hyperfine levels are addressed by sideband modulations of the pumping and repumping lasers [20], and the problem induced by the Zeeman dark state has been solved by either adding an angled static magnetic field [20] or using the so-called switching scheme [22,32]. Another point is the loss channel via the metastable Δ state to even parity $N = 0,2$ rotational states, which could be remixed into the optical cycling with microwave dressing, as performed in YO experiments [23].

Extending the laser-cooling technique to more polar molecules is a challenging and popular topic in physics. The BaF molecule is a promising candidate. The involved transitions have wavelengths around 900 nm (see Fig. 1) in the good regime of the diode laser. It is easy to get a high-power laser for low cost, making the laser-cooling experiments much simpler. Here we consider the feasibility for laser cooling and trapping of a BaF molecule. First, the electronic excited $A^2\Pi_{1/2}$ state has a short lifetime of $\tau \sim 56$ ns (the natural linewidth $\Gamma \approx 2\pi \times 3$ MHz) [33], which enables large photon-scattering rates. Meanwhile, our calculation on the FCFs of the $X^2\Sigma^+_{1/2} \leftrightarrow A^2\Pi_{1/2}$ transition shows that BaF indeed possesses the common highly diagonal feature; see details in Sec. II. Since the BaF molecule has the metastable Δ state, for sideband modulation and microwave remixing considerations, we employed an effective Hamiltonian to obtain the energy values of the spin-rotation and hyperfine levels in the $X^2\Sigma$ state, and further propose a sideband modulation and microwave addressing scheme in Sec. III. According to the magneto-optical trapping designs for SrF and YO [21,22], we calculate the branching ratios from Zeeman sublevels in $A^2\Pi_{1/2}$ to those in the X state, g factors for each hyperfine level, and Zeeman splittings under the external magnetic field; see Secs. IV and V, respectively. In Sec. VI, the metastable Δ state has been investigated in detail due to the possible decay to other even-parity rotational states. We mainly focus on the mixings with $A^2\Pi_{1/2,3/2}$ states and the branching ratios to vibrational states in the X ground state. Section VII gives a brief conclusion to this work.

II. LASER-COOLING SCHEME AND FRANCK-CONDON FACTORS FOR A-X TRANSITION

The BaF molecule has similar electronic structures to SrF [20] and YO [34], and so does the laser-cooling scheme, as

*chentao1990@outlook.com
†yanbohang@zju.edu.cn

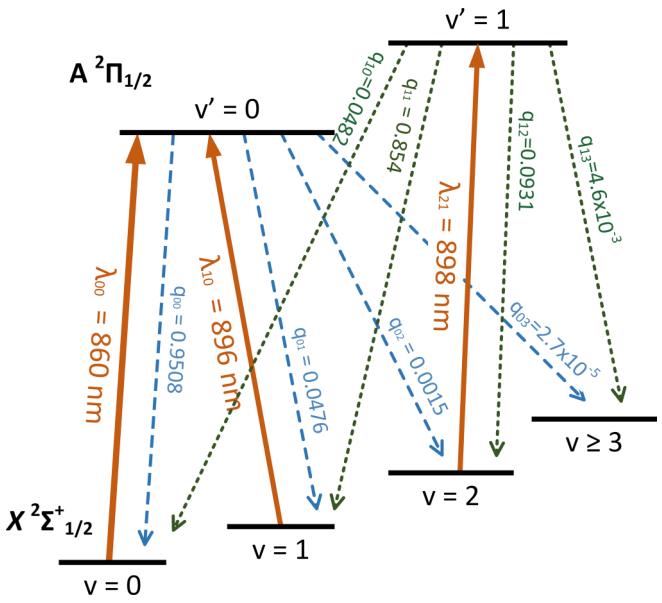

FIG. 1. Vibrational branching is suppressed to achieve a quasicycling transition for the laser-cooling BaF molecule. The orange lines indicate the transitions driven by the cooling laser λ_{00} and the repumping lasers λ_{10}, λ_{21}. The blue and green lines indicate the spontaneous decays from $A\,(v'=0$ and $v'=1)$ to vibrational states in X, respectively. $q_{v'v}$ represents the FCFs for the transition $|A,v'\rangle \rightarrow |X,v\rangle$.

shown in Fig. 1. The quasicycling transition here temporarily takes no consideration on the Δ state, which will be discussed in Sec. VI. Suppression of vibrational branching requires highly diagonal FCFs for $A \rightarrow X$ transitions. We have performed a careful calculation of the FCFs: First, we numerically modeled the potential-energy curves of the lower-lying Σ, Δ, and Π states with the parameters listed in Table I by employing the RKR (Rydberg-Klein-Rees) method [35]. We checked the RKR potential curves with the analytical Morse potentials and found that they are almost the same, especially at the region near the equilibrium positions. Then we used the symplectic propagation method to solve the Schödinger equation and meanwhile make an eigenenergy correction to the trial energy, $E = \omega_e(v+1/2) - \omega_e\chi_e(v+1/2)^2$; see Ref. [36] for more details. After getting the wave functions of each vibrational state, we finally calculate the overlap integrals $\tilde{q}_{v'v} = \langle v'|v\rangle$ and FCFs $q_{v'v} = |\langle v'|v\rangle|^2$, where $|v\rangle$ is the vibrational wave function.

TABLE I. Parameters of the lower-lying electronic states of the ^{138}BaF molecule from previous experimental data [34]. The T_e and splitting constant A_e result in consistent values of T_e in Ref. [38]. The ω_e and $\omega_e\chi_e$ values for the $\Pi_{1/2,3/2}$ and $\Delta_{3/2,5/2}$ doublets have a little difference; see Ref. [38] for details. All values here are in units of cm^{-1}.

	$X^2\Sigma$	$A'^2\Delta$	$A^2\Pi$
T_e	0	10940.27	11962.174
A_e		206.171	632.409
α_A		0.966	−0.5068
ω_e	469.4161	437.41	437.899
$\omega_e\chi_e$	1.83727	1.833	1.854
$\alpha_e \times 10^3$	1.163575	1.2052	1.2563
B_e	0.21652967	0.210082	0.212416

TABLE II. Accurate calculated wavelength values for the cooling and repumping lasers in Fig. 1. The values are generated with the T_e, A_e values in Table I and the calculated eigenenergy values for the corresponding vibrational states. The experimental wavelength for λ_{00} is derived from the measured spectroscopy data in Ref. [37].

Transitions	Calculated (nm)	From experiment (nm)
λ_{00}	859.8415	859.8392
λ_{10}	895.6908	
λ_{21}	897.9117	
λ_{32}	900.1674	

The related values are shown in Fig. 1. Since the $|A,v'=0\rangle \rightarrow |X,v\geqslant 3\rangle$ branching is $q_{03} = 2.7\times10^{-5}$, we use the $|X,v=0\rangle \rightarrow |A,v'=0\rangle$ transition as the main pumping, and the $|X,v=1\rangle \rightarrow |A,v'=0\rangle$ and $|X,v=2\rangle \rightarrow |A,v'=1\rangle$ transitions as the repumpings to achieve $\sim 3\times10^4$ photon scattering before molecules populate the $|X,v\geqslant 3\rangle$ levels. The wavelengths are $\lambda_{00}=860$, $\lambda_{10}=896$, and $\lambda_{21}=898$ nm, respectively. The more accurate wavelength values are listed in Table II. In particular, the experimental value for λ_{00} is derived from the measured spectroscopy data [37]. The difference between our calculation and the experimental value is as small as 0.0316 cm^{-1} (less than 1 GHz). In future experiments, a repumping laser for $|X,v=3\rangle \rightarrow |A,v'=2\rangle$ might be preferred to enhance the photon scattering, just like the three-dimensional (3D) magneto-optical trapping experiment of SrF [21].

Table III lists the FCFs $q_{v'v}$ for vibrational transitions from $A^2\Pi_{1/2}$ and $A^2\Pi_{3/2}$ to $X^2\Sigma_{1/2}$, respectively. Since the parameters ω_e and $\omega_e\chi_e$ for $A^2\Pi_{1/2}$ and $A^2\Pi_{3/2}$ states are nearly the same [38], the corresponding values of the calculated FCFs have no significant differences with each other. The angular momentum selection rules forbid the electronic dipole transitions in $A'^2\Delta \rightarrow X^2\Sigma_{1/2}$, the Δ state

TABLE III. The calculated FCFs ($q_{v'v}$) for vibrational transitions in $|A^2\Pi_{1/2},v'\rangle \rightarrow |X^2\Sigma_{1/2},v\rangle$ and $|A^2\Pi_{3/2},v'\rangle \rightarrow |X^2\Sigma_{1/2},v\rangle$ using the RKR potentials.

$A^2\Pi_{1/2}$, $v' \rightarrow X,v$	$v'=0$	$v'=1$	$v'=2$	$v'=3$	$v'=4$
$v=0$	0.9508	0.0483	9.1×10^{-4}	1.9×10^{-6}	4.5×10^{-7}
$v=1$	0.0476	0.8539	0.0956	0.0030	1.3×10^{-5}
$v=2$	1.5×10^{-3}	0.0925	0.7581	0.1412	0.0065
$v=3$	2.7×10^{-5}	5.1×10^{-3}	0.1347	0.6643	0.1841
$v=4$	4.6×10^{-7}	1.3×10^{-4}	0.0104	0.1733	0.5738
$A^2\Pi_{3/2}$ $v' \rightarrow X,v$	$v'=0$	$v'=1$	$v'=2$	$v'=3$	$v'=4$
$v=0$	0.9508	0.0482	9.7×10^{-4}	3.8×10^{-6}	2.1×10^{-7}
$v=1$	0.0476	0.8539	0.0956	0.0032	2.2×10^{-5}
$v=2$	1.6×10^{-3}	0.0928	0.7582	0.1404	0.0068
$v=3$	2.9×10^{-5}	4.8×10^{-3}	0.1352	0.6648	0.1828
$v=4$	3.7×10^{-7}	1.2×10^{-4}	0.0099	0.1743	0.5746

decays back to the X state via its mixing with the Π states, and thus we do not list the FCFs here. The branching ratios for the spontaneous emissions from A' to X will be discussed in Sec. VI.

III. HYPERFINE STRUCTURES

Now let us consider the rotational branchings. The $X^2\Sigma_{1/2}$ state is a Hund's case (b) state and the rotational quantum number N is a good quantum number, but for the Hund's case (a) state $A^2\Pi_{1/2}$, the good quantum number is $J = N + \Omega$ coupled by the rotational and electronic angular momentum. The $|A^2\Pi_{1/2}, J' = 1/2\rangle$ state has a double orbital degeneracy [39], that is, Λ-doubling structures corresponding to odd- and even-parity electronic wave functions, respectively. Following the parity and angular momentum selection rules for the dipole transition, the parities of the initial and final states should be opposite and $\Delta J = 0, \pm 1$. Consequently, driving $|X, N = 1, -\rangle \rightarrow |A, J' = 1/2, +\rangle$ transitions results in only allowing decays back to $N = 1$, as shown in Fig. 2.

However, the hyperfine structures of both the ground X and excited A states should be taken into account for optical pumping; otherwise the dark states exist. For the Hund's case (a) state $A^2\Pi_{1/2}$, the Λ splitting for the J state with different parity is $\delta E_\Lambda = -(p + 2q)(J + 1/2)$, where $p + 2q = -0.25755\ \mathrm{cm}^{-1}$ for ^{138}BaF [37], while the hyperfine splitting between $F' = 0$ and $F' = 1$ for $|J' = 1/2, +\rangle$ is still unresolved. For ground state $X^2\Sigma^+_{1/2}$, both the spin-rotation and hyperfine interactions split the $|X, N = 1, -\rangle$ state into four components, as shown in Fig. 2. All four hyperfine levels should be pumped simultaneously to prevent molecules from accumulating into one state. To implement the sideband modulation, we have to calculate the relatively precise energy splittings of the hyperfine states in each rotational state of $X^2\Sigma_{1/2}$. The effective Hamiltonian contains the molecular rotational term H_R, the spin-rotational coupling H_{SR}, and the

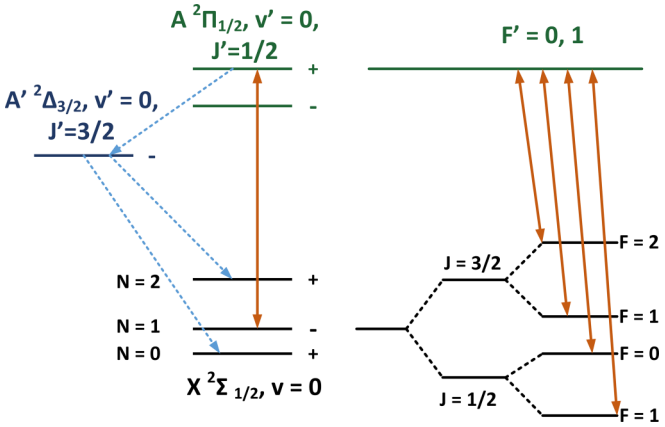

FIG. 2. Rotational branching is eliminated by driving $|X^2\Sigma_{1/2}, N = 1, -\rangle \rightarrow |A^2\Pi_{1/2}, J' = 1/2, +\rangle$ transition. Unfortunately, $|A^2\Pi_{1/2}, J' = 1/2, +\rangle$ can also decay to the $|A'^2\Delta_{3/2}, J' = 3/2, -\rangle$ state, and then back to the $|X, N = 0, 2, +\rangle$ rotational states, which will break the optical cycling. In addition, the $|X, N = 1, -\rangle$ state obeys Hund's case (b) and suffers from spin-rotation and hyperfine splitting, and thus the optical cycling should address all possible levels. Here, $+$ $(-)$ indicates even (odd) parity.

TABLE IV. The Dunham coefficients Y (from Ref. [40]), the spin-rotational constants γ (from Ref. [41]), and the hyperfine constants b,c (from Ref. [42]) used in the hyperfine structure calculation for the ^{138}BaF molecule. All values here are in units of MHz.

Parameters	Values	Parameters	Values
Y_{01}	6491.3946	γ_{00}	80.9840
Y_{02}	-5.5248×10^{-3}	γ_{10}	-58.4×10^{-3}
Y_{11}	-34.8784	γ_{01}	0.112×10^{-3}
Y_{12}	-9.7632×10^{-6}	b_0	63.509
Y_{21}	13.0288×10^{-3}	c_0	8.224

hyperfine interaction H_{hfs}, and is given by

$$\begin{aligned} H_{eff} &= H_R + H_{SR} + H_{hfs}, \quad H_R = B_v\hat{N}^2 - D_v\hat{N}^4, \\ H_{SR} &= \gamma_{vN} T^1(\hat{S})\, T^1(\hat{N}), \\ H_{hfs} &= b_F T^1(\hat{I})\, T^1(\hat{S}) + c_v T^1_{q=0}(\hat{I}) T^1_{q=0}(\hat{S}) \\ &\quad + C_{vN} T^1(\hat{I})\, T^1(\hat{N}), \end{aligned} \tag{1}$$

in which the rotational constant $B_v = Y_{01} + Y_{11}(v + 1/2) + Y_{21}(v + 1/2)^2$, centrifugal distortion constant $D_v = -Y_{02} - Y_{12}(v + 1/2)$, spin-rotational constant $\gamma_{vN} = \gamma_{00} + \gamma_{10}(v + 1/2) + \gamma_{01}N(N + 1)$, Fermi contact constant $b_F = b_v + c_v/3$ with hyperfine constant b_v and dipole-dipole constant c_v, and the nuclear spin-rotational constant C_{vN} is generally small enough, at the magnitude of kilohertz, to be neglected in our calculations, but listed here for completeness. The required Dunham coefficients and γ, b_v, c_v parameters are listed in Table IV.

Since the good quantum numbers for the Hund's case (b) state $X^2\Sigma_{1/2}$ are N, J, F, we expand the Hamiltonian (1) under the basis $|\phi\rangle = |N, S, J, I, F, m_F\rangle$. The corresponding matrix elements for each term of (1) are

$$\begin{aligned} \langle\phi'|B_v\hat{N}^2 - D_v\hat{N}^4|\phi\rangle &= \delta_{N'N}\delta_{J'J}\delta_{F'F}\delta_{m'_F m_F}\{B_v N(N+1) \\ &\quad - D_v[N(N+1)]^2\}, \end{aligned} \tag{2}$$

$$\begin{aligned} &\langle\phi'|\gamma_{vN} T^1(\hat{S})\, T^1(\hat{N})|\phi\rangle \\ &= \delta_{N'N}\delta_{J'J}\delta_{F'F}\delta_{m'_F m_F}\gamma_{vN}(-1)^{N+J+S}\{S\}^{1/2}\{N\}^{1/2} \\ &\quad \times \begin{Bmatrix} S & N & J \\ N & S & 1 \end{Bmatrix}, \end{aligned} \tag{3}$$

$$\begin{aligned} &\langle\phi'|b_F T^1(\hat{I})\, T^1(\hat{S})|\phi\rangle \\ &= \delta_{N'N}\delta_{F'F}\delta_{m'_F m_F} b_F(-1)^{J'+F+I+J+N+1+S}[J']^{1/2}[J]^{1/2} \\ &\quad \times \{S\}^{1/2}\{I\}^{1/2}\begin{Bmatrix} I & J' & F \\ J & I & 1 \end{Bmatrix}\begin{Bmatrix} J & S & N \\ S & J' & 1 \end{Bmatrix}, \end{aligned} \tag{4}$$

$$\begin{aligned} &\langle\phi'|c_v T^1_{q=0}(\hat{I}) T^1_{q=0}(\hat{S})|\phi\rangle \\ &= \delta_{N'N}\delta_{F'F}\delta_{m'_F m_F}(-\sqrt{30}c_v/3)(-1)^{J'+F+I+N}[J']^{1/2}[J]^{1/2} \\ &\quad \times \{S\}^{1/2}\{I\}^{1/2}(2N+1)\begin{pmatrix} N & 2 & N \\ 0 & 0 & 0 \end{pmatrix}\begin{Bmatrix} I & J' & F \\ J & I & 1 \end{Bmatrix} \\ &\quad \times \begin{Bmatrix} J & J' & 1 \\ N & N & 2 \\ S & S & 1 \end{Bmatrix}, \end{aligned} \tag{5}$$

$$\langle\phi'|C_{vN} T^1(\hat{I})\, T^1(\hat{N})|\phi\rangle$$

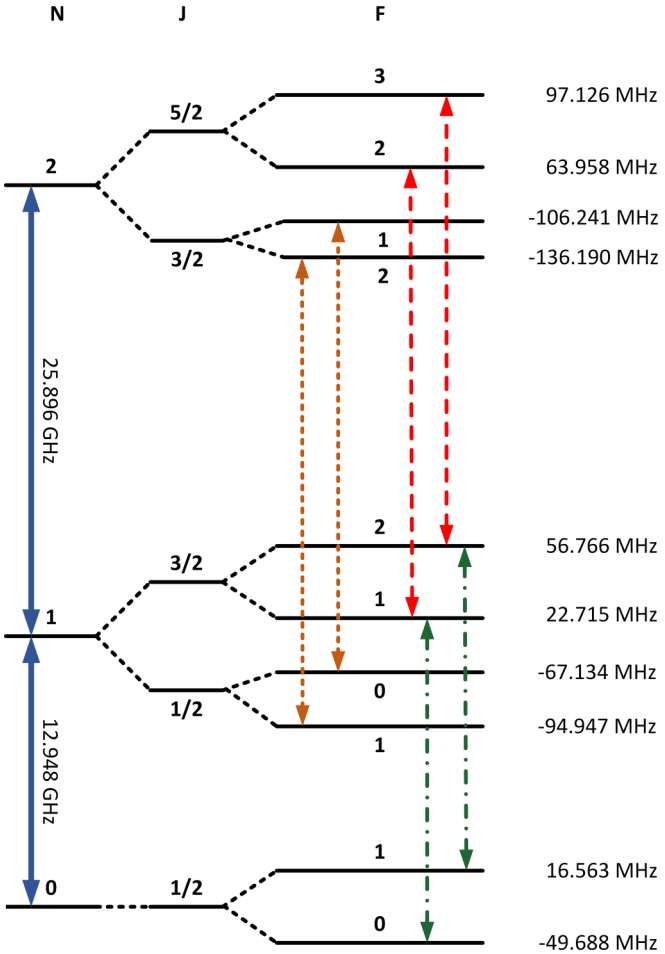

FIG. 3. The spin-rotational splittings and hyperfine levels for $N = 0,1,2$ rotational states in $X^2\Sigma(v = 0)$. The energy values are shown corresponding to the reference energy of each rotational state. The red dashed, orange dotted, and green dot-dashed lines indicate the $\Delta J = +1, \Delta F = +1$ transitions, and the calculated values are listed in Table V, respectively.

$$= \delta_{N'N}\delta_{F'F}\delta_{m'_F m_F} C_{vN}(-1)^{2J+F'+I+N'+1+S}[J']^{1/2}[J]^{1/2} \times \{N\}^{1/2}\{I\}^{1/2}\begin{Bmatrix} I & J & F' \\ J' & I & 1 \end{Bmatrix}\begin{Bmatrix} N & J & S \\ J' & N' & 1 \end{Bmatrix}, \quad (6)$$

where $[x]^{1/2} = \sqrt{2x+1}$ and $\{x\}^{1/2} = \sqrt{x(x+1)(2x+1)}$.

By diagonalizing the H_{eff} matrix, the energy splittings between different rotational hyperfine levels are obtained and illustrated in Fig. 3. The data therein is for the $v = 0$ case, while for higher $v = 1,2$ states, the energy splittings differ very little (~kHz level) from those of $v = 0$ because the γ_{10} is about several tens of kHz. Based on the calculated data, we first discuss the sideband modulation to the pumping (λ_{00}) and repumping ($\lambda_{10}, \lambda_{21}$) lasers for $|X, N = 1, F\rangle \leftrightarrow |A, J' = 1/2, F' = 0,1\rangle$ transitions. Figure 4 shows the theoretically calculated fluorescence spectra and the proposed sideband frequency distributions generated by an electro-optical modulator (EOM). By simply choosing the laser detuning $\delta = -20$ MHz and the modulating frequency $f_{\text{Mod}} = 40$ MHz, the four hyperfine levels of $N = 1$ are all addressed with detunings within 3Γ, respectively. Here the laser detuning δ is defined by

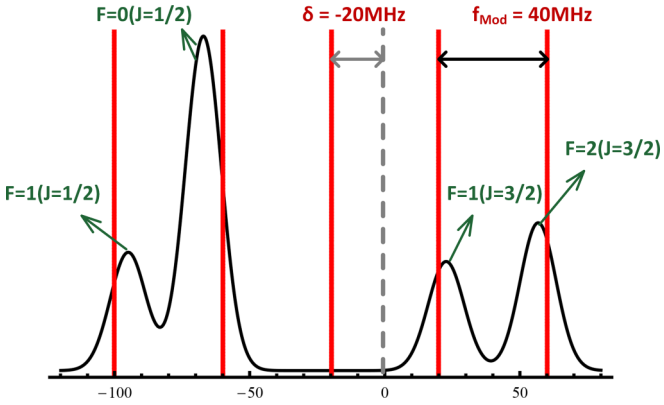

FIG. 4. The proposed sideband modulation scheme to the (re)pumping lasers to simultaneously cover all four hyperfine levels of $|X, N = 1\rangle$. The calculated spectra (black line) are plotted with the branching ratio from the $|A, J = 1/2, +\rangle$ to each hyperfine level (see Fig. 2) as the strength of each peak, the calculated energy value in Fig. 3 as the center frequency, and Γ as the linewidth. The vertical solid red line indicates the sidebands of an EOM. By simply making the laser detuning $\delta = -20$ MHz and the modulated frequency $f_{\text{Mod}} = 40$ MHz, the resultant sideband frequency values are matched within $\sim 3\Gamma$ detuned to the respective peaks.

the frequency difference to the $|X, N = 1\rangle \leftrightarrow |A, J' = 1/2\rangle$ transition, while in SrF experiments [20,21], the laser detuning is experimentally determined to be zero when a maximal laser-induced fluorescence signal is obtained, and this zero value in turn serves as a benchmark to define the laser detunings.

On the other hand, different from the SrF molecule, an additional feature of BaF is the leakage decay to $|X, N = 0,2, +\rangle$ states via the metastable Δ state (see Fig. 2), which leads to the unexpected rotational branchings. Fortunately, a microwave remixing method could solve this problem [23,43]. In Fig. 3, the energy splittings for rotational states and all hyperfine states are shown. Here we plan to use the $\Delta J = +1, \Delta F = +1$ transitions to implement the microwave remixing, and the corresponding frequency values are listed in Table V. We have compared our calculated values with the experimentally observed spectra data in Ref. [42] and found that the differences are within several kHz. Such small difference also

TABLE V. Comparison of the calculated and experimentally observed transition frequencies for $\Delta J = J' - J = +1, \Delta F = F' - F = +1$ hyperfine transitions in rotational states of the $X^2\Sigma_{1/2}$ state of BaF. The frequency difference $\Delta f = f_{\text{calc}} - f_{\text{obs}}$ is defined. The experimental data is taken from Ref. [42].

$N' - N$	$J' - J$	$F' - F$	f_{calc} (MHz)	f_{obs} (MHz)	Δf (kHz)
$1 - 0$	$3/2 - 1/2$	$1 - 0$	13020.2976	13020.286	+11.6
		$2 - 1$	12988.0986	12988.110	−11.4
$2 - 1$	$3/2 - 1/2$	$1 - 0$	25856.5501	25865.572[a]	
		$2 - 1$	25854.4139	25854.434	−20.0
	$5/2 - 3/2$	$2 - 1$	25936.9012	25936.873	+28.2
		$3 - 2$	25936.0181	25936.006	+12.1

[a]This value in Ref. [42] has a significant difference from our calculated value.

demonstrates the reliability of our calculations from another side. Microwave radiation tuned to $f_0 = 12948 \pm 15$ MHz can drive $|N=0,F=0\rangle \leftrightarrow |N=1,J=1/2,F=0\rangle$ and $|N=0,F=1\rangle \leftrightarrow |N=1,J=3/2,F=1\rangle$ transitions to mix the $N=0$ hyperfine states with those in $N=1$, while the $N=2$ is remixed to $N=1$ just by doubling the frequency f_0 to drive $\Delta J=+1, \Delta F=+1$ transitions. The detunings for the six transitions are less than 10 MHz.

At this point, we have discussed the quasiclosed optical cycling for the BaF molecule in detail over all directions: the short lifetime of the $A^2\Pi_{1/2}$ state, highly diagonal FCFs, parity selection rules and microwave remixing assisted rotational branching elimination, as well as sideband modulation to address all four hyperfine levels of $|X,N=1\rangle$. In the following sections, we mainly focus on the molecular properties correlated with the magneto-optical trapping experiment, including the branching ratios, the energy splittings under the external field, and the lifetime estimation of the δ state.

IV. BRANCHING RATIOS FOR *A*-*X* TRANSITION

The branching ratios reflect the distributions of the transition strengths for all possible hyperfine decay paths. It is therefore necessary to calculate the branching ratios to determine the required laser intensities for certain transitions and for reproducing the molecular population distribution with experimentally observed line strengths to these hyperfine levels. In this section, we summarize the calculation details of the hyperfine branching ratios in the $A-X$ transition for BaF following the derivations in Ref. [44].

Before deriving the matrix elements for the electric dipole transition in $A-X$, we first investigate the J mixing of the hyperfine levels in the ground X state, where spin-rotation interaction produces J splittings and then hyperfine interaction results in different F branchings. The mixing coefficients are obtained by diagonalizing the $H_{\rm eff}$ matrix; see Eq. (1). For $N=0$, $J=1/2$, no mixing exists, while for $N=1$ or $N=2$ manifold, the hyperfine levels with the same F value, but in different J components, suffer from the so-called J mixing. Here we still label the nominal mixed hyperfine level as $|N,J,F\rangle$, but the pure J state as $|N,J(F)\rangle$. The mixing situations for $N=1$ and $N=2$ are shown in Table VI. Knowledge of J mixing is required in the following branching ratio calculations.

TABLE VI. The J-mixing phenomena in $N=1$ and $N=2$ rotational states of the ground X state. The corresponding coefficients are $\alpha_1 = 0.9593, \beta_1 = 0.2824$ and $\alpha_2 = 0.9858, \beta_2 = 0.1679$.

N	Mixed label	Superposition of pure J states
1	$\|J=1/2,F=0\rangle$	$\|J=1/2(F=0)\rangle$
	$\|J=1/2,F=1\rangle$	$\alpha_1\|J=1/2(F=1)\rangle + \beta_1\|J=3/2(F=1)\rangle$
	$\|J=3/2,F=1\rangle$	$-\beta_1\|J=1/2(F=1)\rangle + \alpha_1\|J=3/2(F=1)\rangle$
	$\|J=3/2,F=2\rangle$	$\|J=3/2(F=2)\rangle$
2	$\|J=3/2,F=1\rangle$	$\|J=3/2(F=1)\rangle$
	$\|J=3/2,F=2\rangle$	$\alpha_2\|J=3/2(F=2)\rangle + \beta_2\|J=5/2(F=2)\rangle$
	$\|J=5/2,F=2\rangle$	$-\beta_2\|J=3/2(F=2)\rangle + \alpha_2\|J=5/2(F=2)\rangle$
	$\|J=5/2,F=3\rangle$	$\|J=5/2(F=3)\rangle$

Now let us discuss the calculation of the branching ratios for all possible hyperfine decays from $|A,J=1/2,+\rangle$ to $|X,N=1,-\rangle$. We first convert the nominal basis sets $|X;N,J,F\rangle$ and $|A;J,+\rangle$ into the Hund's case (a) basis $|\Lambda,S,\Sigma,\Omega,J,I,F,m_F\rangle$. The nominal J-mixed $|N,J,F\rangle$ states in X can be written as superpositions of pure J states $|\Lambda;N,S,J(F)\rangle$ (abbreviated as $|N,J(F)\rangle$ in Table VI). The pure J state is the Hund's case (b) state and can further be converted to the Hund's case (a) basis as

$$|\Lambda;N,S,J(F)\rangle = \sum_{\Omega}\sum_{\Sigma}(-1)^{J+\Omega}\sqrt{2N+1} \times \begin{pmatrix} S & N & J \\ \Sigma & \Lambda & -\Omega \end{pmatrix} |\Lambda,S,\Sigma,\Omega,J,F\rangle, \quad (7)$$

while for the A state,

$$||\Lambda|,J,\pm\rangle = \frac{1}{\sqrt{2}}(|\Lambda;S,\Sigma;J,\Omega\rangle \pm(-1)^{J-S}|-\Lambda;S,-\Sigma;J,-\Omega\rangle). \quad (8)$$

Then we calculate the matrix element for the electric dipole transition between two Zeeman sublevels labeled as $|\psi_e\rangle$ and $|\psi_g\rangle$ under the Hund's case (a) basis, that is,

$$\begin{aligned}\langle d\rangle &= \langle\psi_e|T^1_p(\hat{d})|\psi_g\rangle \\ &= \left\langle\alpha_e;J_e,I_e,F_e,m_{F,e}\middle|T^1_p(\hat{d})\middle|\alpha_g;J_g,I_g,F_g,m_{F,g}\right\rangle \\ &= (-1)^{F_e-m_{F,e}+F_g+J_e+I_g+1}[F_e]^{1/2}[F_g]^{1/2} \\ &\quad\times\begin{pmatrix} F_e & 1 & F_g \\ -m_{F,e} & p & m_{F,g}\end{pmatrix}\begin{Bmatrix} J_g & F_g & I_g \\ F_e & J_e & 1\end{Bmatrix} \\ &\quad\times\langle\alpha_e;J_e||T^1(\hat{d})||\alpha_g;J_g\rangle, \end{aligned} \quad (9)$$

where $|\alpha\rangle = |\Lambda;S,\Sigma;\Omega\rangle$. Applying the Wigner-Eckart theorem to the last term in Eq. (9), we obtain

$$\begin{aligned}&\langle\Lambda_e;S_e,\Sigma_e;\Omega_e,J_e||T^1(\hat{d})||\Lambda_g;S_g,\Sigma_g;\Omega_g,J_g\rangle \\ &= \sum_{q=-1}^{1}(-1)^{J_e-\Omega_e}[J_e]^{1/2}[J_g]^{1/2}\begin{pmatrix} J_e & 1 & J_g \\ -\Omega_e & q & \Omega_g\end{pmatrix} \\ &\quad\times\langle\Lambda_e;S_e,\Sigma_e||T^1_q(\hat{d})||\Lambda_g;S_g,\Sigma_g\rangle, \end{aligned} \quad (10)$$

where $\Sigma_e = \Sigma_g$ should be satisfied since the electrical dipole operator $T^1_q(\hat{d})$ can change neither the electron spin nor the spin projection, and the matrix element $\langle\Lambda_e||T^1_q||\Lambda_g\rangle$ is common for all $\Delta\Lambda = \pm 1$ transitions.

Putting Eqs. (7)–(10) and the formula in Table VI all together, the branching ratios for decays from hyperfine Zeeman sublevels in $|A,J=1/2,+\rangle$ to those in the $|X,N=1,-\rangle$ state are obtained and summarized in Table VII. Besides, the branching ratios for transitions in $|A,J=1/2,-\rangle \rightarrow |X,N=0,2,+\rangle$ are listed in Table VIII. The calculated branching ratios provide instructive directions for future laser-cooling and trapping experiments on the BaF molecule.

V. ZEEMAN SPLITTINGS UNDER MAGNETIC FIELD

To achieve the remixing of the dark Zeeman sublevels [21] and further trapping of molecules [22,32], an external magnetic field is usually applied to the molecules. In a magneto-optical

TABLE VII. Calculated hyperfine branching ratios for decays from the $|A, J' = 1/2, +\rangle$ state to the $|X, N = 1, -\rangle$ state. The line strengths in Fig. 4 are estimated with the values here.

			$F' = 0$		$F' = 1$	
J	F	m_F	$m'_F = 0$	$m'_F = -1$	$m'_F = 0$	$m'_F = 1$
1/2	0	0	0	2/9	2/9	2/9
		−1	0.2985	0.1641	0.1641	0
1/2	1	0	0.2985	0.1641	0	0.1641
		1	0.2985	0	0.1641	0.1641
		−1	0.0348	0.0859	0.0859	0
3/2	1	0	0.0348	0.0859	0	0.0859
		1	0.0348	0	0.0859	0.0859
		−2	0	1/6	0	0
		−1	0	1/12	1/12	0
3/2	2	0	0	1/36	1/9	1/36
		1	0	0	1/12	1/12
		2	0	0	0	1/6

trap, the magnetic field is employed to create a position-dependent restoring force to cool and confine the atoms or molecules. The degeneracy of the total $2F + 1$ Zeeman sublevels for a state labeled by quantum number F is broken by the external magnetic field. In this section, we focus on the Zeeman splittings of the two states involved with the cooling transition, $|X, N = 1, -\rangle \leftrightarrow |A, J = 1/2, +\rangle$. Under the external field B_z, the Zeeman Hamiltonian,

$$H_z = \left[g_S \mu_B T^1_{p=0}(\hat{S}) + g_L \mu_B T^1_{p=0}(\hat{L}) - g_I \mu_N T^1_{p=0}(\hat{I})\right] B_z, \tag{11}$$

together with the spin-rotation and hyperfine interaction terms in Eq. (1) contribute to the splittings of the Zeeman sublevels. For the ground state $|X, N = 1, -\rangle$, the three terms in Hamiltonian H_z are expanded under the basis $|\phi\rangle = |N, S, J, I, F, m_F\rangle$, respectively, as

$$\begin{aligned}
&\langle \phi | g_S \mu_B T^1_{p=0}(\hat{S}) | \phi' \rangle \\
&= g_S \mu_B (-1)^{F - m_F} \begin{pmatrix} F & 1 & F' \\ -m_F & 0 & m'_F \end{pmatrix} (-1)^{F' + J + 1 + I} \\
&\quad \times [F']^{1/2} [F]^{1/2} (-1)^{J' + N + 1 + S} [J']^{1/2} [J]^{1/2} \{S\}^{1/2} \\
&\quad \times \begin{Bmatrix} F & J & I \\ J' & F' & 1 \end{Bmatrix} \begin{Bmatrix} J & S & N \\ S & J' & 1 \end{Bmatrix},
\end{aligned} \tag{12}$$

$$\begin{aligned}
&\langle \phi | g_L \mu_B T^1_{p=0}(\hat{L}) | \phi' \rangle \\
&= g_L \mu_B (-1)^{F - m_F} \begin{pmatrix} F & 1 & F' \\ -m_F & 0 & m'_F \end{pmatrix} (-1)^{F' + J + 1 + I} \\
&\quad \times [F']^{1/2} [F]^{1/2} (-1)^{J' + N + 1 + S} [J']^{1/2} [J]^{1/2} (-1)^{N - \Lambda} \\
&\quad \times [N]^{1/2} [N']^{1/2} \begin{Bmatrix} F & J & I \\ J' & F' & 1 \end{Bmatrix} \begin{Bmatrix} J & N & S \\ N' & J' & 1 \end{Bmatrix} \\
&\quad \times \begin{pmatrix} N & 1 & N' \\ -\Lambda & 0 & \Lambda \end{pmatrix} \Lambda,
\end{aligned} \tag{13}$$

and

$$\begin{aligned}
&\langle \phi | g_I \mu_B T^1_{p=0}(\hat{I}) | \phi' \rangle \\
&= g_I \mu_N \delta_{J, J'} (-1)^{F - m_F} \begin{pmatrix} F & 1 & F' \\ -m_F & 0 & m'_F \end{pmatrix} (-1)^{F' + J + 1 + I} \\
&\quad \times [F']^{1/2} [F]^{1/2} \{I\}^{1/2} \begin{Bmatrix} F & I & J \\ I & F' & 1 \end{Bmatrix}.
\end{aligned} \tag{14}$$

Since $\Lambda = 0$ for the $X^2\Sigma$ state, the second term (13) vanishes; and the third term (14) is sufficiently smaller to be able to be neglected due to $\mu_B/\mu_N \approx 1836$. Consequently, the effective Hamiltonian matrix is constructed by the elements from Eqs. (3)–(5) and (12). By diagonalizing the matrix at different magnetic field strengths, we obtain the Zeeman energy splittings as shown in Fig. 5. The splitting behaviors at weak and strong magnetic field strengths show different features. In the strong-field region, the sublevels with different F, m_F values totally split.

However, the typical magneto-optical trap for molecules employs a field of only about several Gauss in strength. When the magnetic field is weak, the Zeeman Hamiltonian is just a perturbation to the hyperfine interaction term, and thus the energy shifts for sublevels in $|J = 3/2, F = 1, 2\rangle$ and $|J = 1/2, F = 0\rangle$ show nearly linear variations, as illustrated in Fig. 5(c). But especially for the $|J = 1/2, F = 1\rangle$ manifold, the shifts do not linearly vary along with the field strengths, that is, the linear region is rather small (less than 5 Gauss); see Fig. 5(b). The reason is that the matrix element of the hyperfine term for $|J = 1/2, F = 1\rangle$ is relatively smaller than those for $|J = 3/2, F = 1, 2\rangle$, and thus much more easily perturbed by the external magnetic field. Another point is that the variation behavior cannot be correctly described by the typical g factors; instead, mixed g factors are used to describe the linear gradients of the Zeeman shifts. By applying a rather small magnetic field strength, say 0.01 Gauss, to the Zeeman Hamiltonian (11), we obtain the energy differences with the degenerate hyperfine levels at zero strength for all

TABLE VIII. Calculated hyperfine branching ratios for decays from the $|A, J' = 1/2, -\rangle$ state to the $|X, N = 0, 2, +\rangle$ state.

				$F' = 0$		$F' = 1$	
N	J	F	m_F	$m'_F = 0$	$m'_F = -1$	$m'_F = 0$	$m'_F = 1$
0	1/2	0	0	0	2/9	2/9	2/9
			−1	2/9	2/9	2/9	0
		1	0	2/9	2/9	0	2/9
			1	2/9	0	2/9	2/9
			−1	1/9	1/36	1/36	0
2	3/2	1	0	1/9	1/36	0	1/36
			1	1/9	0	1/36	1/36
			−2	0	0.1620	0	0
			−1	0	0.0810	0.0810	0
	3/2	2	0	0	0.0270	0.1080	0.0270
			1	0	0	0.0810	0.0810
			2	0	0	0	0.1620
			−2	0	0.0047	0	0
			−1	0	0.0023	0.0023	0
	5/2	2	0	0	0.0008	0.0031	0.0008
			1	0	0	0.0023	0.0023
			2	0	0	0	0.0047

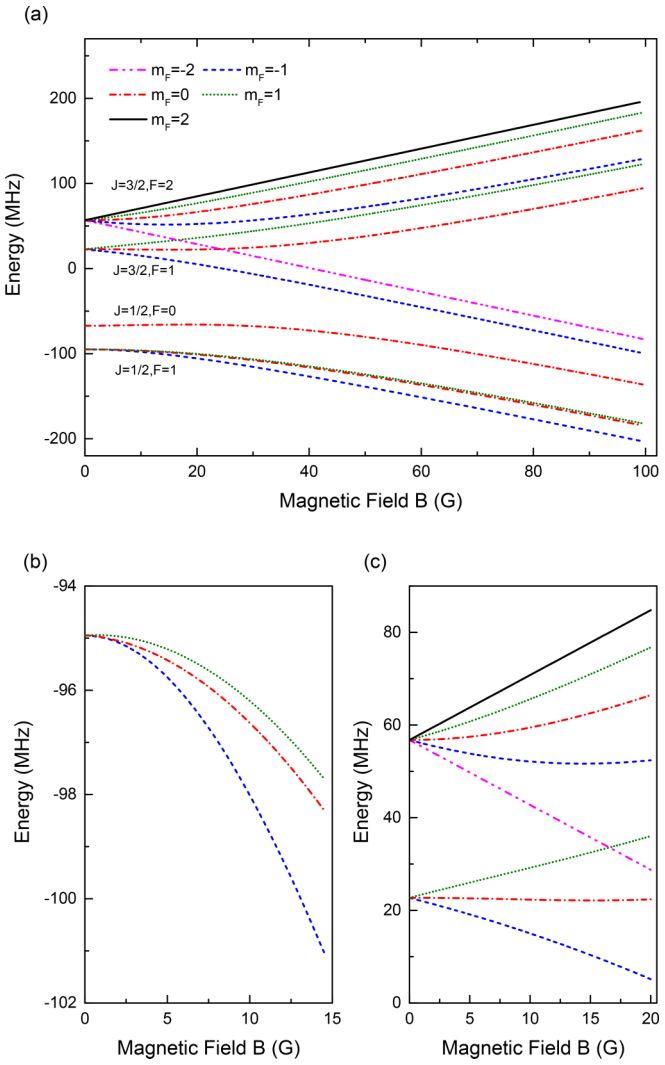

FIG. 5. Zeeman splittings for sublevels in the four hyperfine states of the $|X,N=1,-\rangle$ manifold. (a) The whole picture, with sublevels labeled by the same m_F quantum number that are plotted in the same line shapes, respectively. (b),(c) Zoom-in plots of $|J=1/2,F=1\rangle$ and $|J=3/2,F=1,2\rangle$ manifolds, respectively, at small magnetic field region.

Zeeman sublevels, and the mixed g factors are yielded by a transformation.

Table IX gives the typical g factors and the mixed g factors for the four hyperfine states in $|X,N=1,-\rangle$. For states $|J=1/2,F=0\rangle$ and $|J=3/2,F=2\rangle$, no J mixing exists, and both of the g factors remain identical with those typical g_F for pure J states. However, the mixed g factors for two $|F=1\rangle$ states change significantly due to the J-mixing effect, which is much stronger than the Zeeman effect from external field. This is different from SrF [21] and MgF [27], where the mixed g factor for $|J=1/2,F=1\rangle$ is negative and an additional opposite polarized trapping laser should be combined; the g factor for BaF here is positive, that is, all hyperfine manifolds have $g>0$ and thus laser addressing different manifolds could take the same polarizations for optimal trapping.

TABLE IX. The typical g factors (g_F) and the mixed ones for the four hyperfine levels in the $|X,N=1,-\rangle$ state.

State label	Typical g factor, g_F	Mixed g factor
$\|J=1/2,F=0\rangle$	0.00	0.000
$\|J=1/2,F=1\rangle$	−0.33	0.015
$\|J=3/2,F=1\rangle$	0.83	0.485
$\|J=3/2,F=2\rangle$	0.50	0.500

However, Tarbutt [45] has pointed out that even for a type-II magneto-optical trap, the restoring force and the laser polarizations are still mainly determined by the g factor of the excited state. Under magnetic field strength B_z, the Zeeman interaction energy for the Hund's case (a) state $|\Lambda;J,\Omega;F,m_F\rangle$ is given by

$$\Delta E_z=\frac{g_L\Lambda+g_s\Sigma}{J(J+1)}\Omega\mu_B B_z m_F, \tag{15}$$

where $g_L\approx 1$, $g_S=2.0023$. For the $|A^2\Pi,J=1/2\rangle$ state, $\Delta E_z=7.7\times10^{-4}\mu_B m_F B_z$. The g factor is close to zero.

Fortunately, the excited $\Pi_{1/2}$ state, in fact, is not totally a pure state, and it is usually spin orbital mixed with an upper $\Sigma_{1/2}$ state, which introduces additional parity-dependent terms to the Zeeman Hamiltonian [46]. According to the derivations in Ref. [46], for the $|A,J=1/2,\pm,F=1\rangle$ state, the parity-dependent Zeeman shift is

$$\Delta E_{pz\pm}=\pm g_p\mu_B m_F B_z, \tag{16}$$

where $-$ and $+$ indicate the odd and even parity, and g_p is derived from Λ-doubling coefficients and the rotational constant [45]. For the BaF molecule in $|A,J=1/2,+,F=1\rangle$, $g_p=\frac{1}{3}(p+2q)/(2B_e)=-0.202$, which is much larger than $g_p=-0.088$ for SrF [47], $g_p=-0.065$ for YO [22], and $g_p=-0.021$ for CaF [48]. The larger g factor of the upper state should result in a larger magneto-optical trapping force, and one can also resort to the rapid switching of the polarization of the trapping laser to achieve a better trapping effect.

VI. THE Δ STATE

In Sec. III, we discussed the undesired leakage decay from $|A,J=1/2,+\rangle$ to $|X,N=0,2,+\rangle$ via the $A'^2\Delta_{3/2}$ state, which will break the quasiclosed optical cycling. One problem of concern for our future laser-cooling experiment is the decay rate from the $|A',J=3/2,-\rangle$ to the $|X,N=0,2,+\rangle$ state, that is, the lifetime of the metastable Δ state. In fact, the Δ state decays back to the X state due to its mixing with the upper $A^2\Pi$ state and the selection rules forbid direct electric dipole transition from Δ to Σ where $\Delta\Lambda=2$. In this section, we focus on the identification of the mixing between the $A'^2\Delta_{3/2}$ and $A^2\Pi$ states, and then make an estimation of the lifetime of the $A'^2\Delta$ state based on the mixing coefficients, just like that performed for the YO molecule [49].

The mixing of the $\Delta_{3/2}$ and $\Pi_{1/2,3/2}$ states originates from the spin-orbit and the rotational electronic Coriolis interactions, denoted as $H_{\rm so}$ and $H_{\rm cor}$, respectively. The spin-orbit operator $H_{\rm so}=\sum_i\sum_{q=\pm1}T^1_q(\hat{a}_i\hat{l}_i)T^1_{-q}(\hat{s}_i)$ describes the total effect from the interaction of each electron's spin ($\hat{s}_i$) with its own motion (described by the angular momentum $\hat{l}_i$), while

the Coriolis operator $H_{\rm cor} = -\frac{\hbar}{4\pi c\mu r^2}\sum_{q=\pm1} T^1_q(\hat{J})T^1_{-q}(\hat{L})$ reflects the effect from the interaction between the electron's motion and molecular rotation. Both of the operators can couple two states with $\Delta\Lambda = \pm1$. The detailed descriptions for the two operators are discussed in Refs. [46,50]. Following the procedure in Ref. [50], the off-diagonal nonzero matrix elements for $H_{\rm so}$ and $H_{\rm cor}$ operators are given as

$$\begin{aligned}
\langle v, A'^2\Delta_{3/2}|H_{\rm cor}|A^2\Pi_{1/2}, v'\rangle &= -\sqrt{3}B_{vv'}b_2,\\
\langle v, A'^2\Delta_{3/2}|H_{\rm cor}|A^2\Pi_{3/2}, v'\rangle &= B_{vv'}b_2,\\
\langle v, A'^2\Delta_{3/2}|H_{\rm so}|A^2\Pi_{3/2}, v'\rangle &= \langle v|v'\rangle a_2,\\
\langle v, A'^2\Pi_{1/2}|H_{\rm cor}|A^2\Pi_{3/2}, v'\rangle &= -\sqrt{3}B_{vv'},
\end{aligned} \tag{17}$$

where $a_2 = A_e^{\Pi}$ (see Table I), $b_2 = 2$ [50], $\langle v|v'\rangle$ is the vibrational wave-function overlap, and $B_{vv'} = \frac{\hbar}{4\pi c\mu}\langle v|(1/r^2)|v'\rangle$ is a vibrational averaging (over internuclear distance r) value. The relevant $\langle v|v'\rangle$ and $B_{vv'}$ values for the $|A'^2\Delta_{3/2}, v = 0,1,2\rangle$, $|A^2\Pi_{1/2}, v = 0,1,2\rangle$, and $|A^2\Pi_{3/2}, v = 0,1,2\rangle$ states are listed in Tables X and XI, respectively. The vibrational wave functions are evaluated with the method in Sec. II.

We construct the Hamiltonian matrix by taking the eigenenergy values of the vibrational states [adding the energy gaps $T_e(\Pi_{3/2}) - T_e(\Delta_{3/2})$ and $T_e(\Pi_{1/2}) - T_e(\Delta_{3/2})$ for the corresponding states in $A^2\Pi_{3/2}$ and $A^2\Pi_{1/2}$] as the diagonal elements. However, the eigenenergy arrays should be eigenvalues of the mixing Hamiltonian matrix, and thus we should vary the diagonal elements one by one to make the eigenvalues of the mixing matrix closer to the eigenenergy values of those states involved step by step. When the eigenvalues are closely approaching each respective eigenenergy for the nine vibrational states, the eigenvector can approximately describe the mixing of the pure Born-Oppenheimer Π and Δ states. For the $v = 0$ state in mixed $A'^2\Delta_{3/2}$, the wave function is given by

$$\begin{aligned}
&|\widetilde{\Delta_{3/2}}, v = 0\rangle\\
&\quad\approx 0.88732|\Delta_{3/2}, v = 0\rangle - 0.45945|\Pi_{3/2}, v = 0\rangle\\
&\qquad - 0.03539|\Pi_{3/2}, v = 1\rangle + 0.00072|\Pi_{3/2}, v = 2\rangle\\
&\qquad + 0.00052|\Pi_{1/2}, v = 0\rangle + \cdots .
\end{aligned} \tag{18}$$

The mixing coefficients here along with the vibrational wave-function overlaps between $A^2\Pi$ and $X^2\Sigma$ can give an approximate estimation of the vibrational branching ratios from the $A'^2\Delta_{3/2}$ to the $X^2\Sigma$ states. For the $|A', v = 0\rangle$ state, about 91.2% decay back to $|X, v = 0\rangle$, 8.3% to $|X, v = 1\rangle$, and the remaining 0.4% to the $|X, v \geqslant 2\rangle$ states. In the actual cooling procedure, rapid decay rates from $|A'^2\Delta_{3/2}, J' = 3/2,-\rangle$ to $|X, N = 0,2,+\rangle$ are required, so the lifetime of the Δ state should not be too long. Considering the 21% mixing with $A^2\Pi_{3/2}$ and that the lifetime of the $A^2\Pi_{3/2}$ state is 46 ns [33], the $A'^2\Delta_{3/2}$ has a lifetime of ~220 ns, which guarantees that after the pumped molecules in the excited $|A^2\Pi_{1/2}, J = 1/2,+\rangle$ state relax to the $|A'^2\Delta_{3/2}, J = 3/2,-\rangle$ state, they can rapidly decay back to the $|X, N = 0,2,+\rangle$ states, and then be remixed back to $|X, N = 1,-\rangle$ in optical cycling by the microwave scheme described in Sec. III.

TABLE X. The vibrational wave function overlaps $\langle v|v'\rangle$ for $A'^2\Delta_{3/2} - A^2\Pi_{1/2}$ and $A'^2\Delta_{3/2} - A^2\Pi_{3/2}$.

		$A'^2\Delta_{3/2}(v)$		
		0	1	2
$A^2\Pi_{3/2}(v')$	0	0.99228	−0.12190	0.02235
	1	0.12401	0.97733	−0.16722
	2	−0.00135	0.17306	0.96321
$A^2\Pi_{1/2}(v')$	0	0.97511	0.21781	0.041001
	1	−0.21962	0.92411	0.30419
	2	0.03027	−0.30913	0.87070

TABLE XI. The $B_{vv'}$ values for $A'^2\Delta_{3/2} - A^2\Pi_{1/2}$, $A'^2\Delta_{3/2} - A^2\Pi_{3/2}$, and $A^2\Pi_{1/2} - A^2\Pi_{3/2}$.

		$A'^2\Delta_{3/2}(v)$		
		0	1	2
$A^2\Pi_{3/2}(v')$	0	0.20904	−0.03477	0.00710
	1	0.01689	0.20466	−0.04771
	2	−0.00102	0.02336	0.20048
$A^2\Pi_{1/2}(v')$	0	0.20904	−0.03473	0.00730
	1	0.01689	0.20467	−0.04761
	2	−0.00125	0.02334	0.20049
		$A'^2\Pi_{3/2}(v)$		
		0	1	2
$A^2\Pi_{1/2}(v')$	0	0.21183	−0.00931	0.00109
	1	−0.00933	0.21057	−0.01306
	2	0.00066	−0.01313	0.20931

VII. CONCLUSION

To conclude, we have investigated the molecular structures and branching ratios for the BaF molecule and further demonstrated the feasibility of laser cooling and trapping. The BaF molecule has both the identical properties with laser-cooled SrF and YO molecules and its own unique character. The short lifetime for the $A^2\Pi_{1/2}$ state, the highly diagonal FCFs, and the microwave remixing of different rotational manifolds in X states implement the quasiclosed optical cycling procedure. Based on our calculations on the hyperfine splittings, we have proposed a sideband modulation scheme to simultaneously pump the four hyperfine levels of $|X, N = 1\rangle$ and an optimal choice of the microwave frequencies. The results of the branching ratios, Zeeman splittings, and g factors will serve as a reference for adjustment of laser powers and polarizations. Finally, we have checked again that the leakage process via the Δ state can be eliminated with microwave remixing since the lifetime of the Δ state is estimated to be about 220 ns. The results and proposed schemes show the feasibility of future laser-cooling and trapping experiments on the BaF molecule.

ACKNOWLEDGMENTS

The authors acknowledge the support from the National Natural Science Foundation of China under Grant No. 91636104, and the Fundamental Research Funds for the Central Universities Grant No. 2016QNA3007.

[1] L. D. Carr, D. DeMille, R. V. Krems, and J. Ye, New J. Phys. **11**, 055049 (2009).

[2] B. Yan, S. A. Moses, B. Gadway, J. P. Covey, K. R. A. Hazzard, A. M. Rey, D. S. Jin, and J. Ye, Nature (London) **501**, 521 (2013).

[3] M. A. Baranov, M. Dalmonte, G. Pupillo, and P. Zoller, Chem. Rev. **112**, 5012 (2012).

[4] S. Ospelkaus, K.-K. Ni, D. Wang, M. H. G. de Miranda, B. Neyenhuis, G. Quéméner, P. S. Julienne, J. L. Bohn, D. S. Jin, and J. Ye, Science **327**, 853 (2010).

[5] D. DeMille, S. B. Cahn, D. Murphree, D. A. Rahmlow, and M. G. Kozlov, Phys. Rev. Lett. **100**, 023003 (2008).

[6] C. Chin, V. V. Flambaum, and M. G. Kozlov, New J. Phys. **11**, 055048 (2009).

[7] D. DeMille, Phys. Rev. Lett. **88**, 067901 (2002).

[8] A. Andre, D. DeMille, J. M. Doyle, M. D. Lukin, S. E. Maxwell, P. Rabl, R. J. Schoelkopf, and P. Zoller, Nat. Phys. **2**, 636 (2006).

[9] K.-K. Ni, S. Ospelkaus, M. H. G. de Miranda, A. Pe'er, B. Neyenhuis, J. J. Zirbel, S. Kotochigova, P. S. Julienne, D. S. Jin, and J. Ye, Science **322**, 231 (2008).

[10] S. A. Moses, J. P. Covey, M. T. Miecnikowski, B. Yan, B. Gadway, J. Ye, and D. S. Jin, Science **350**, 659 (2015).

[11] B. Gadway and B. Yan, J. Phys. B **49**, 152002 (2016).

[12] J. R. Bochinski, E. R. Hudson, H. J. Lewandowski, G. Meijer, and J. Ye, Phys. Rev. Lett. **91**, 243001 (2003).

[13] E. Narevicius, A. Libson, C. G. Parthey, I. Chavez, J. Narevicius, U. Even, and M. G. Raizen, Phys. Rev. Lett. **100**, 093003 (2008).

[14] R. Fulton, A. I. Bishop, M. N. Shneider, and P. F. Barker, Nat. Phys. **2**, 465 (2006).

[15] R.-Q. Liu, Y.-L. Yin, and J.-P. Yin, Chin. Phys. B **21**, 033302 (2012).

[16] M. Zeppenfeld, M. Motsch, P. W. H. Pinkse, and G. Rempe, Phys. Rev. A **80**, 041401 (2009).

[17] A. Prehn, M. Ibrügger, R. Glöckner, G. Rempe, and M. Zeppenfeld, Phys. Rev. Lett. **116**, 063005 (2016).

[18] M. D. Di Rosa, Eur. Phys. J. D - At. Mol. Opt. Plas. Phys. **31**, 395 (2004).

[19] B. K. Stuhl, B. C. Sawyer, D. Wang, and J. Ye, Phys. Rev. Lett. **101**, 243002 (2008).

[20] E. S. Shuman, J. F. Barry, and D. DeMille, Nature (London) **467**, 820 (2010).

[21] J. F. Barry, D. J. McCarron, E. B. Norrgard, M. H. Steinecker, and D. DeMille, Nature (London) **512**, 286 (2014).

[22] M. T. Hummon, M. Yeo, B. K. Stuhl, A. L. Collopy, Y. Xia, and J. Ye, Phys. Rev. Lett. **110**, 143001 (2013).

[23] M. Yeo, M. T. Hummon, A. L. Collopy, B. Yan, B. Hemmerling, E. Chae, J. M. Doyle, and J. Ye, Phys. Rev. Lett. **114**, 223003 (2015).

[24] V. Zhelyazkova, A. Cournol, T. E. Wall, A. Matsushima, J. J. Hudson, E. A. Hinds, M. R. Tarbutt, and B. E. Sauer, Phys. Rev. A **89**, 053416 (2014).

[25] B. Hemmerling, E. Chae, A. Ravi, L. Anderegg, G. K. Drayna, N. R. Hutzler, A. L. Collopy, J. Ye, W. Ketterle, and J. M. Doyle, J. Phys. B: At. Mol. Opt. Phys. **49** 174001 (2016).

[26] I. Smallman, F. Wang, T. Steimle, M. Tarbutt, and E. Hinds, J. Mol. Spectrosc. **300**, 3 (2014).

[27] L. Xu, Y. Yin, B. Wei, Y. Xia, and J. Yin, Phys. Rev. A **93**, 013408 (2016).

[28] R. J. Hendricks, D. A. Holland, S. Truppe, B. E. Sauer, and M. R. Tarbutt, Front. Phys. **2**, 51 (2014).

[29] T. A. Isaev, S. Hoekstra, and R. Berger, Phys. Rev. A **82**, 052521 (2010).

[30] L. R. Hunter, S. K. Peck, A. S. Greenspon, S. S. Alam, and D. DeMille, Phys. Rev. A **85**, 012511 (2012).

[31] M. G. Tarallo, G. Z. Iwata, and T. Zelevinsky, Phys. Rev. A **93**, 032509 (2016).

[32] E. B. Norrgard, D. J. McCarron, M. H. Steinecker, M. R. Tarbutt, and D. DeMille, Phys. Rev. Lett. **116**, 063004 (2016).

[33] L.-E. Berg, N. Gador, D. Husain, H. Ludwigs, and P. Royen, Chem. Phys. Lett. **287**, 89 (1998).

[34] A. Bernard, C. Effantin, E. Andrianavalona, J. Vergus, and R. Barrow, J. Mol. Spectrosc. **152**, 174 (1992).

[35] A. L. G. Rees, Proc. Phys. Soc. **59**, 998 (1947).

[36] T. Chen, S. Zhu, X. Li, J. Qian, and Y. Wang, Phys. Rev. A **89**, 063402 (2014).

[37] T. C. Steimle, S. Frey, A. Le, D. DeMille, D. A. Rahmlow, and C. Linton, Phys. Rev. A **84**, 012508 (2011).

[38] R. Barrow, A. Bernard, C. Effantin, J. D'Incan, G. Fabre, A. E. Hachimi, R. Stringat, and J. Vergés, Chem. Phys. Lett. **147**, 535 (1988).

[39] R. S. Mulliken and A. Christy, Phys. Rev. **38**, 87 (1931).

[40] B. Guo, K. Zhang, and P. Bernath, J. Mol. Spectrosc. **170**, 59 (1995).

[41] C. Ryzlewicz and T. Torring, Chem. Phys. **51**, 329 (1980).

[42] W. E. Ernst, J. Kändler, and T. Törring, J. Chem. Phys. **84**, 4769 (1986).

[43] D. Xie, W. Bu, and B. Yan, Chin. Phys. B **25**, 053701 (2016).

[44] T. E. Wall, J. F. Kanem, J. J. Hudson, B. E. Sauer, D. Cho, M. G. Boshier, E. A. Hinds, and M. R. Tarbutt, Phys. Rev. A **78**, 062509 (2008).

[45] M. R. Tarbutt, New J. Phys. **17**, 015007 (2015).

[46] J. Brown and A. Carrington, *Rotational Spectroscopy of Diatomic Molecules* (Cambridge University Press, Cambridge, 2003).

[47] T. C. Steimle, P. J. Domaille, and D. O. Harris, J. Mol. Spectrosc. **73**, 441 (1978).

[48] J. Nakagawa, P. J. Domaille, T. C. Steimle, and D. O. Harris, J. Mol. Spectrosc. **70**, 374 (1978).

[49] A. L. Collopy, M. T. Hummon, M. Yeo, B. Yan, and J. Ye, New J. Phys. **17**, 055008 (2015).

[50] C. L. Chalek and J. L. Gole, J. Chem. Phys. **65**, 2845 (1976).